Journal of the Optical Society of America B
OPTICAL PHYSICS

Gain in europium-chelate-doped polymer-optical-fiber amplifiers

J. Arrue,[1,*] B. García-Ramiro,[1] F. Jiménez,[1] M. A. Illarramendi,[1] I. Ayesta,[1] J. Zubia,[1] R. Evert,[2] and D. Zaremba[2]

[1]Escuela de Ingeniería de Bilbao, University of the Basque Country (UPV/EHU), Plaza Ingeniero Torres Quevedo, 1, E48013 Bilbao, Spain
[2]Labor für Elektrooptik am Institut für Hochfrequenztechnik, TU Braunschweig, Bienroder Weg 94, D38106 Braunschweig, Germany
*Corresponding author: jon.arrue@ehu.eus

Received 25 July 2018; revised 18 September 2018; accepted 18 September 2018; posted 20 September 2018 (Doc. ID 340672); published 11 October 2018

A model of partial differential rate equations for the analysis of signal gain in typical europium-chelate-doped polymer optical fibers is presented and solved by a method of finite differences. The qualitative reliability of some of the results is confirmed by means of a simplified analytical expression. Typical types of chelates at various concentrations are studied in order to be able to optimize the fiber length and pumping conditions for attainment of maximum signal gain. © 2018 Optical Society of America

OCIS codes: (130.5460) Polymer waveguides; (160.5690) Rare-earth-doped materials; (060.2270) Fiber characterization; (060.2320) Fiber optics amplifiers and oscillators; (230.4480) Optical amplifiers; (060.4510) Optical communications.

https://doi.org/10.1364/JOSAB.35.002770 Provided under the terms of the OSA Open Access Publishing Agreement

1. INTRODUCTION

In the last few decades, there have been continual advances in the performance of polymer optical fibers (POFs), whose interest over glass fibers lies in that they provide several distinctive features such as a large fiber diameter, easiness of handling and of light coupling, or suitability for working in the visible region of the spectrum [1]. Also, POFs are manufactured at much lower temperatures, which facilitates the incorporation of active dopants during the manufacturing process [2,3]. For this reason, POFs can be doped with organic dyes or with rare-earth organic complexes, some of which can generate or amplify visible light at the low-attenuation windows of POFs [4,5]. Emission and absorption properties of these dopants can be employed to achieve luminescence enhancement in the visible region by pumping the POF appropriately, which is interesting for diverse types of applications [5–9]. As a consequence, research on doped POFs is on an upward trend, and the results obtained are being applied for the development of solar concentrators that collect and transport solar light [5,6], for the design of optical amplifiers [8], and also for the manufacture of superluminiscent speckle-free light sources based on the phenomenon of amplified spontaneous emission (ASE) [7–10].

In the case of optical amplifiers, the desired range of emission wavelengths for the dopant usually lies in the blue, green, or red regions of the spectrum, where the attenuation of typical commercial POFs is lower due to the proximity of the attenuation windows of the main constituent material of the fiber core, namely, poly(methyl methacrylate) (PMMA) [8]. When working in these windows, the corresponding coefficients of attenuation in commercial undoped POFs are often lower than two tenths of dB/m (e.g., around 0.18 dB/m in the red), which allows attenuation-limited distances above 100 m [11]. However, achievable distances sometimes fall short of what is desired for some local area networks (LANs). Even in the case of more sophisticated perfluorinated graded-index POFs, whose attenuation coefficient is usually lower than 0.05 dB/m [12], light amplification may also be needed for some LANs in order to compensate for losses in optical devices such as splitters, apart from losses along the fiber. This task can be carried out by inserting a short length of doped POF into the POF link. The specific dopant is chosen in view of some important features such as the values of its absorption and emission cross sections at the pump and signal wavelengths [13,14], respectively. These values should be large for the sake of compactness. In addition, the dopant must be soluble in the core material during the manufacturing process. Both conditions are fulfilled in the case of organic-dye-doped POFs, which have been the primary focus of many research works [13–18]. However, organic dyes have a serious problem of photodegradation, since emission drops progressively due to continual exposure to the pump light [9]. In contrast, lanthanides such as europium, which emits in the red, are free from photodegradation [4,19]. Nevertheless, europium does not dissolve in the PMMA of the fiber, and the absorption cross section

of europium atoms is too low for the manufacture of compact devices. For these reasons, europium is inserted into chelates, which are molecules in which a central europium ion is attached by coordinate bonds to a few identical absorbing ligands and a neutral ligand that does not take place in the absorption [20–25]. Europium chelates are not only soluble in a PMMA POF, but they also allow efficient absorption of pump energy, which affects the europium ion in an indirect way, via an energy-transfer process from each absorbing ligand [26]. Accordingly, europium chelates were the first substances employed for the achievement of laser phenomena in the liquid phase [27], although the necessary pump energy of the pump pulses was very high (>1000 J). However, using a POF instead of bulk material serves to reduce pump energy dramatically, owing to the long interaction length between the emitted power and pump power, in addition to the high light energy density that is achieved inside the fiber core.

In 1993, the first POF amplifier was reported. It was prepared by doping an organic dye (rhodamine B) into a POF [28]. Since then, several theoretical or experimental studies of the optical properties of POFs or polymer waveguides doped with rare-earth organic complexes or with europium chelates emitting in the red have been reported [29–33,21]. The feasibility of amplifying an optical signal by means of such devices was also confirmed experimentally (5.7 dB of gain using a moderate pump energy density of 3 mJ/mm^2) [30].

In this paper, we model the amplification of light in POFs doped with typical europium chelates. For this purpose, several processes must be taken into account. These are (1) absorption of ultraviolet or violet pump light by a ligand of the europium ion, (2) energy transfer from the ligand to the ion, and (3) emission of red light by the ion. Each absorbing ligand may be involved in various transitions and energy transfers. These can vary from one Eu^{3+} chelate to another, and their values condition the achievable quantum yield, which is the number of red photons emitted by the Eu^{3+} ion per photon of incident pump radiation. Consequently, diverse europium complexes have been prepared by several research groups, in an attempt to improve quantum yield [22,23,34], but the information corresponding to all the rates for a specific Eu^{3+} complex is usually not available, due to the difficulty in determining them accurately. The transition and transfer rates employed for the theoretical calculations in this paper correspond to coordination complexes of high quantum yield. Our computational results obtained with such rates also predict a small positive gain for the same moderate pump energy density as that utilized in Ref. [30] for experimental confirmation of gain in a similar doped POF.

Our simulations are made with samples doped with two different europium complexes at various concentrations, in order to facilitate drawing conclusions. One of the main contributions of our work is that we model the system as a three-energy-level one, taking into account the propagation and attenuation in an optical fiber. This serves to complement previous models reported for similar types of systems in which the europium was in powder in random lasers instead of in an optical fiber [10]. It also constitutes a more accurate description than previous models in which a two-level approach was employed, instead of our three-level one with intercrossing both towards and from the europium ion [20]. Another contribution is that we derive a simplified analytical expression that serves to model the evolution of the generated power as it propagates, while the pump power is still non-negligible. The attenuation of generated light in the red region is also taken into account, and its effect is studied as well. Moreover, the values of spectral attenuation used for the simulations are obtained from our own experimental measurements of the samples analyzed.

2. BACKGROUND THEORY

The model implemented in this paper can be utilized for any typical type of europium chelate that might be used for the development of POF amplifiers, because all of these types can be modeled by means of the same basic energy-transition diagram. The set of energy levels and the transitions considered or neglected in our model are depicted in Fig. 1.

As can be observed in this figure, the pump power excites the ligand from its ground singlet state S_0 to its singlet state S_1, from where it undergoes a non-radiative decay to its triplet state T, by means of a process known as intersystem crossing [22,23]. In turn, a ligand in its excited state T can lose its energy through a relatively slow decay to S_0, or, alternatively, through an intramolecular energy transfer to the Eu^{3+} ion. In the figure, we have depicted three possible energy-transfer processes from each ligand to the europium ion: from S_1 to $^5D_4$, from T to $^5D_1$ (at rate W_{ET1}), and from T to $^5D_0$ (at rate W_{ET0}). However, any energy transfer from S_1 to the europium ion can be neglected, because the population of ligands in state S_1 is negligible as compared to the population of ligands in the triplet state T, owing to the very rapid pace at which the intersystem crossings from S_1 to T occur. Simultaneously, there are back energy transfers from level $^5D_1$ of europium to T (at rate W_{BT}), but it can be assumed that there are not significant back energy transfers from $^5D_0$ to T, because $^5D_0$ is located at a considerably lower energy

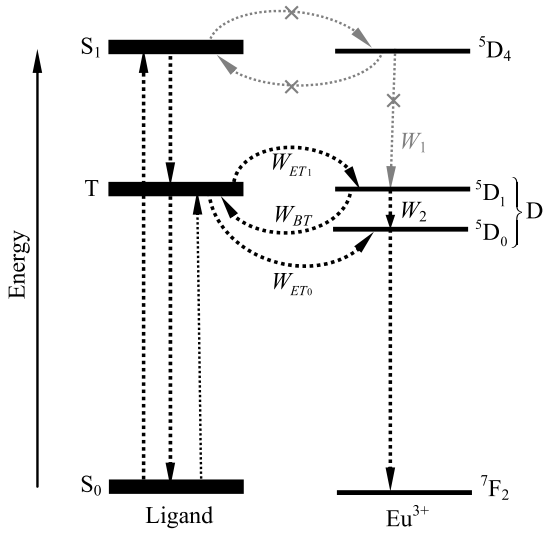

Fig. 1. Energy levels and transitions of typical coordination complexes of Eu^{3+}.

than T. There are also non-radiative decays from $^5D_1$ to $^5D_0$ (at rate W_2).

For the calculations in this paper, the two levels $^5D_1$ and $^5D_0$ will be merged into a single level D. In doing so, both energy transfers from T to D, which occur at rates W_{ET1} and W_{ET0} as depicted in the figure, are also merged into a single one, which occurs at a rate $W_{ET} = W_{ET1} + W_{ET0}$ transitions/s. On the other hand, the rate W_{BT} from $^5D_1$ to T is typically much greater than the rate W_2 from $^5D_1$ to $^5D_0$, so $W_{BT} + W_2 \approx W_{BT}$, which means that only W_2 transitions out of approximately W_{BT} go to $^5D_0$ every second, while the rest of the transitions go to T. Therefore, the quotient W_2/W_{BT} indicates the fraction by which the population of our merged level D does not contribute to the transitions from D to T. Similarly, the fraction by which this population contributes to the transitions from D to T is $1 - W_2/W_{BT}$, which is a number very close to 1 when W_2 is much lower than W_{BT}.

Photon emission occurs when any europium ion at level D decays radiatively to one of its ground levels $^7F_0$, $^7F_1$, $^7F_2$, $^7F_3$ or $^7F_4$, thus yielding five emission peaks. However, the peak corresponding to the $^5D_0 \rightarrow {}^7F_2$ transition, which is centered at about 613–614 nm, clearly dominates all the other peaks for typical europium complexes, as will be shown in Section 3. Therefore, we need to consider only one emission wavelength, λ_s, and one pump wavelength, λ_p. Power generated at λ_s will be called P, and the pump power will be P_p. The number of europium ions in the excited energy level D per unit volume will be N_D. Similarly, N_T will be the population of excited ligands. The number of dopant molecules per unit volume is N, so the populations of non-excited europium ions and non-excited ligands are, respectively, $N - N_D$ and $N - N_T$. There are typically three or more absorbing ligands in each molecule of europium complex, apart from a neutral ligand that is not involved in the absorption. However, all the absorbing ligands are identical, so only one needs to be considered in the rate equations, which can be written as follows:

PUMP-POWER PROPAGATION:

$$\frac{\partial P_p}{\partial z} = \underbrace{-\sigma^a (N - N_T) P_p}_{\text{absorption}} - \underbrace{\frac{1}{v_z}\frac{\partial P_p}{\partial t}}_{\text{propagation}}, \tag{1}$$

RATE EQUATION FOR N_D:

$$\frac{\partial N_D}{\partial t} = \underbrace{\frac{-N_D}{\tau_{D-F}}}_{\text{spontaneous decay}} \underbrace{-\frac{\sigma^e}{h\frac{c}{\lambda_s}A_{\text{core}}} N_D P}_{\text{stimulated decay}} + \underbrace{W_{ET}\frac{N - N_D}{N} N_T}_{\text{energy transfer from } T} \underbrace{- W_{BT}\frac{N - N_T}{N}(1 - W_2/W_{BT}) N_D}_{\text{energy transfer from } D}, \tag{2}$$

GENERATED-POWER PROPAGATION:

$$\frac{\partial P}{\partial z} = \underbrace{\sigma^e N_D P}_{\text{stimulated emission}} + \underbrace{\frac{N_D}{\tau_{D-F}} h \frac{c}{\lambda_s} \beta A_{\text{core}}}_{\text{spontaneous emission}} - \underbrace{\frac{1}{v_z}\frac{\partial P}{\partial t}}_{\text{propagation}} - \underbrace{\alpha P}_{\text{attenuation at } \lambda_s}, \tag{3}$$

RATE EQUATION FOR N_T:

$$\frac{\partial N_T}{\partial t} = \underbrace{-\frac{N_T}{\tau_{T-S_0}}}_{\text{spontaneous decay}} + \underbrace{\frac{\sigma^a}{h\frac{c}{\lambda_p}A_{\text{core}}}(N - N_T) P_p}_{\text{absorption}} \underbrace{- W_{ET}\frac{N - N_D}{N} N_T}_{\text{energy transfer from } T} + \underbrace{W_{BT}\frac{N - N_T}{N} N_D}_{\text{energy transfer to } T}. \tag{4}$$

In these equations, t is the elapsed time, and z is the traveled distance along the direction of the fiber symmetry axis. τ_{T-S0} and τ_{D-F} represent the decay lifetimes from T to S_0 and from D to $^7F_2$, respectively. σ^e is the emission cross section of the dopant at λ_s, whereas σ^a (measured at λ_p) is the absorption cross section of the dopant. A_{core} is the area of the cross section of the fiber core, h is Planck's constant, and c is the speed of light in vacuum. β stands for the fraction of spontaneously generated photons that are emitted in guided directions towards the output end of the fiber with respect to the number of photons emitted in all directions. It can be calculated from the expression $\beta = (n_1 - n_2)/(2n_1)$, where n_1 and n_2 are the refractive indices of the core and the cladding, respectively [8]. In terms that represent the propagation of light, v_z is the speed of light in the fiber core, i.e., c/n_1. In Eq. (3), α is the attenuation coefficient of the emitted light. As for the absorption of pump light in Eq. (1), it can be considered to be due to the absorption by the dopant exclusively, which is much higher than the absorption by the PMMA at any of the typically employed pump wavelengths. These are located in the regions of high attenuation coefficient (which will be shown in Fig. 3). The population N_T may also increase, albeit in a nearly negligible way, due to transitions caused by the very weak absorption of the ligand at the emission wavelength of the europium ion, as will be shown in Section 3. In any case, these absorption transitions are of secondary importance.

Equations (2) and (4) have been derived from those reported in Refs. [26,35], where the rate equations were written taking only time into account, because they used only samples of europium complexes in bulk. An optical fiber requires the introduction of an additional spatial variable, namely, position z, and the addition of two more Eqs. (1) and (3), in order to take into account the variations of P_p and P with z [8]. Boundary conditions are that $P_p(t, z = 0)$ is a Gaussian pulse and that $P(t, z = 0)$ is a Gaussian signal centered at the same time as the pump pulse. The fiber extends from $z = 0$ to $z = L$. Numerical values of the parameters employed for the calculations will be shown in Section 4.

The four rate equations have been solved by means of finite differences. More specifically, we have employed the following approximations:

$$\frac{\partial P_p}{\partial t}(i+1,j) \approx \frac{P_p(i+1,j) - P_p(i,j)}{dt},$$
$$\frac{\partial P_p}{\partial z}(i+1,j) \approx \frac{P_p(i+1,j+1) - P_p(i+1,j)}{dz},$$
$$\frac{\partial N_T}{\partial t}(i,j+1) \approx \frac{N_T(i+1,j+1) - N_T(i,j+1)}{dt},$$
$$\frac{\partial N_D}{\partial t}(i,j+1) \approx \frac{N_D(i+1,j+1) - N_D(i,j+1)}{dt},$$
$$\frac{\partial P}{\partial t}(i+1,j) \approx \frac{P(i+1,j) - P(i,j)}{dt},$$
$$\frac{\partial P}{\partial z}(i+1,j) \approx \frac{P(i+1,j+1) - P(i+1,j)}{dz}.$$

In this way, we can calculate the four variables P, P_p, N_T, and N_D at the point $(i+1, j+1)$ in terms of values at the points (i, j), $(i, j+1)$, and $(i+1, j)$.

3. EXPERIMENTAL MEASUREMENTS

The europium complexes analyzed are known as AC46 and AC56, which are, respectively, shorthand terms for Tris(1, 1, 1, 5, 5, 5 - hexafluor - 2, 4 - pentandion - κO_2, κO_4) [4′ - (4 - phenoxymethacrylat) - 2, 2′:6′, 2″ - terpyridin - κN_1, $\kappa N_{1'}$, $\kappa N_{1''}$] europium(III), and Tris[1 - (2thienyl) - 4, 4, 4 - trifluor - 1, 3 - butandion - κO_1, κO_3] [4′ - (4 - phenoxymethacrylat) - 2, 2′:6′, 2″ - terpyridin - κN_1, $\kappa N_{1'}$, $\kappa N1''$] europium(III). As can be seen in Fig. 2, both structures differ only in the type of the saturation ligand. These are hexafluoroacetylacetone for AC46 and 4, 4, 4 - Trifluoro - 1 - (2 - thienyl) - 1, 3 - butanedione for AC56. Thereby the thienyl group in the AC56 saturation ligands acts as an electron donor, which leads to a bathochromic shift in the absorption wavelength.

The calculations in this paper were carried out for three different POF samples. One of the POFs was doped with the europium complex AC46 at a concentration of 50 parts per million in weight (ppm), or 0.005 mol%; another sample was also doped with AC46 but at a concentration of 500 ppm (0.05 mol%), and another sample was doped with the europium complex AC56 at a concentration of 500 ppm (0.05 mol%). The spectral attenuation curves of these samples were measured by means of a Perkin Elmer Lambda 9 UV/VIS/NIR spectrometer, in arbitrary units. Absolute values of such curves were determined by measuring the attenuation coefficients at two wavelengths (633 nm and 379 nm) using the cut-back technique for each of the samples. The resulting attenuation coefficients are shown in Fig. 3. Absolute values measured at these two wavelengths fitted well with the relative shape provided by the spectrometer within a margin of error of about 20%. The value of σ^a (measured at λ_p) was derived from these attenuation curves.

The details of the equipment utilized are as follows. The 633 nm light source was a Thorlabs HNL 150L He–Ne laser whose emission power was 45 mW. This light was first launched into a longer fiber of 6.64 m and, afterwards, into a shorter one of 2.58 m. The 379 nm light source was a Spectra-Physics laser diode whose output power would have been 8 mW, but it was diminished by means of a Newport optical density filter that reduced the power at this wavelength by a factor of 40, in order to avoid fluorescence as much as possible. In this case, the light was first launched into a longer fiber of 13 cm and, afterwards, into a shorter one of 6.5 cm. In all cases, the fiber ends were smoothed by cutting them with a blade and sanding them with polishing papers of progressively smaller grains. The detector used was a Newport 2936-R with the photodiode Newport 818-UV.

As for the emission of europium, our experimental measurements confirmed that the fluorescence spectrum presents a dominant peak at about 613–614 nm for the two dopants considered (Fig. 4). Fluorescence spectra were recorded on an Agilent Technologies (Santa Clara, CA, USA) Cary Eclipse G9800A fluorescence spectrophotometer working with Cary Eclipse WinFLR software v.1.2 with the following settings: slit width of 5 nm, medium detector voltage, 1 nm resolution, and medium scanning speed. These measurements were made from solid pieces obtained from the preforms. They were side illuminated with a spot size of around 2 mm and very low energy density due to the halogen lamp of the spectrometer. The sample length was about 15 mm. The source and the detector in

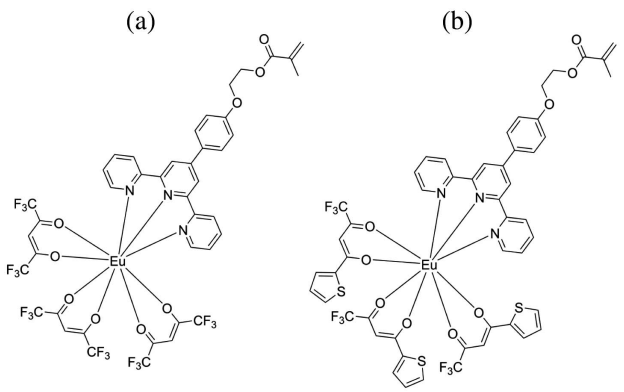

Fig. 2. Europium complexes (a) AC46 and (b) AC56.

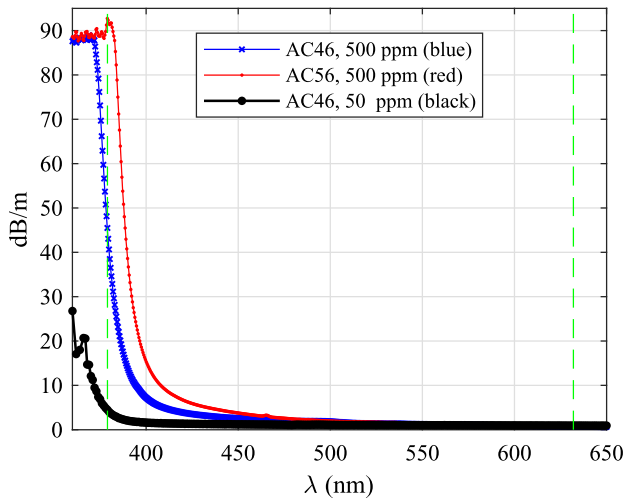

Fig. 3. Spectral attenuation coefficients for three POF samples doped with different europium complexes or with different concentrations. The relative shapes were provided by a spectrometer, and absolute values were estimated from measurement of the attenuation of light launched from a He–Ne laser ($\lambda = 633$ nm) and also from a 379 nm laser diode, by using the cut-back technique in both cases.

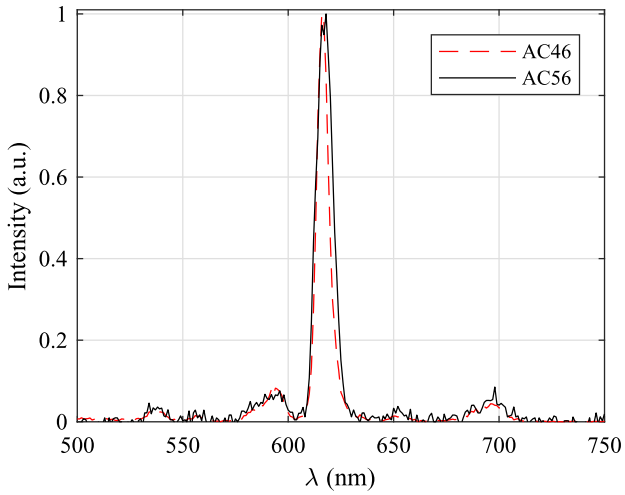

Fig. 4. Normalized fluorescence spectra of two typical europium complexes (AC46 and AC56) pumped at 350 nm, measured by the authors from the preforms of the 500 ppm doped fibers.

the device were placed at an angle of 45°. Emission was taken from the illuminated surface of the sample.

4. SIMULATION PARAMETERS FOR CALCULATION OF SIGNAL GAIN

The parameters that appear in our four rate equations are summarized in Table 1 for a typical europium-chelate-doped POF amplifier [22,26,30]. The reference pump energy density is a moderate one (3 mJ/mm^2) that serves to achieve signal gain [30]. Since this paper studies the influence of varying some adjustable parameters (fiber length, dopant concentration, and pumping) by analyzing changes in the results rather than absolute results, the conclusions reported here can be expected to be generalizable to fibers doped with any other similar europium complex. In all the simulations, the launched pump power is a Gaussian pulse. Its full width at half maximum (FWHM) and its peak power ($P_{p\,\max}$) can be easily proved to be related to pulse energy E_p through the following formula: $E_p = P_{p\,\max} \cdot \mathrm{FWHM} \cdot 1.066$.

Table 1. Simulation Parameters for a Typical Europium-Chelate-Doped POF Amplifier

Simulation Parameters	Units	Value
σ^a	m^2	$3.45 \cdot 10^{-23}$
σ^e	m^2	$4.64 \cdot 10^{-24}$
λ_p	m	$379 \cdot 10^{-9}$
λ_s	m	$614 \cdot 10^{-9}$
τ_{T-S0}	s	$1.0 \cdot 10^{-5}$
τ_{D-F}	s	$1.02 \cdot 10^{-3}$
W_2	s^{-1}	10^6
W_{ET}	s^{-1}	$8 \cdot 10^8$
W_{BT}	s^{-1}	$2 \cdot 10^8$
A_{core}	m^2	$1.257 \cdot 10^{-7}$
β	non-dimensional	0.025
v_z	m/s	$2 \cdot 10^8$
P maximum at $z = 0$	W	0.2
Fiber length (L)	m	≥ 0.3
Signal full width at half max.	ns	200
P_p maximum at $z = 0$	W	23.7
Pump full width at half max.	µs	To be optimized
Pump energy	J	$0.379 \cdot 10^{-3}$
Pump energy density	mJ/mm^2	3

Even though this pump energy usually has a strong influence on signal gain, it also holds that there is an optimum temporal pump width that maximizes signal gain. In the next section we will determine the optimum temporal pump width corresponding to the parameters in Table 1. Signal gain can be calculated as the quotient between the area of the output signal over the ASE baseline and the area of the input signal, as shown in Fig. 5.

For determination of optimum pulse width, let us consider a range of values of the FWHM between, e.g., 10 µs and 2000 µs. Therefore, we need to simulate from an initial time of 0 µs to a final time of about 6400 µs in order to be able to accommodate the whole Gaussian pump pulse inside the range of simulated times. The required time of computation depends on the step sizes in $t(\delta t)$ and in $z(\delta z)$. The following values have proved to result in numerical stability: $\delta t = 0.8 \cdot 10^{-9}$ s and $\delta z = 200 \cdot 10^{-6}$ m. Therefore, the program would need to complete 1500 steps in z and 8 million steps in t for each point of the graph, which is done in about 120 min in our 16 GB, 1600 MHz computer. The simulation program was written in the *Julia* programming language, which was chosen because of its speed while being at the same time a high-level programming language that we find very convenient for scientific computing.

In a first set of results, we will simulate a fiber with a higher concentration of Eu chelate, namely, 4000 ppm, which is the concentration employed in the experimental results of [30].

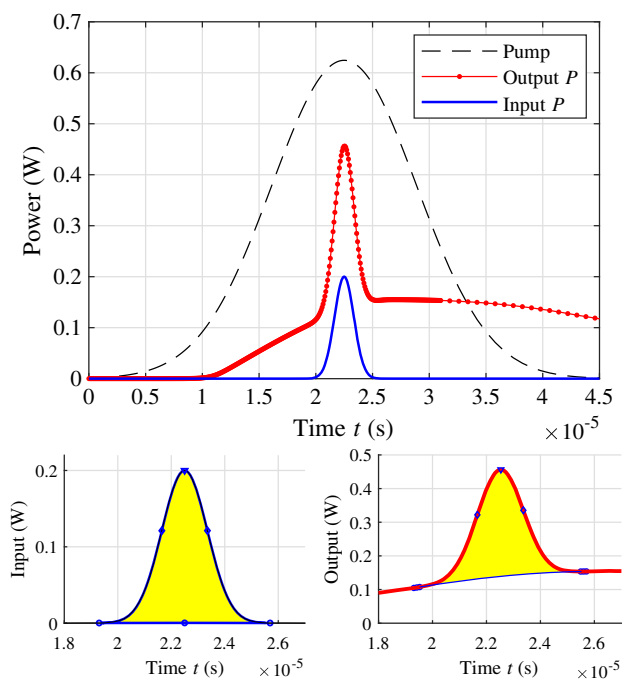

Fig. 5. Calculation of signal gain as the quotient between the area of the output signal over the ASE baseline and the area of the input signal. General parameters as in Table 1. Fiber length: $L = 0.3$ m.

In a second stage, concentrations will be lower for the sake of comparison.

5. THEORETICAL RESULTS AND DISCUSSION

Figure 6 shows signal gain as a function of the width of the pump pulse using the parameters shown in Table 1, for a fiber doped at a concentration of 4000 ppm. A positive gain, on the same order of magnitude as that measured in Ref. [30], is obtained with the same moderate pump energy density. The attenuation coefficient α at the signal wavelength has been assumed to be 1 dB/m. Other values of α would change the results slightly, as will be shown later. The maximum gain achieved theoretically is 4.1 dB. As can be seen in the figure, optimum FWHM in our case is about 15 μs, and the gain decreases significantly when the pump width is increased to values comparable to the decay time $\tau_{D\text{-}F}$ of the europium ion. This can be easily understood by taking into account that, at any point z of the fiber, spontaneous decay prevents population inversion found by the signal from being affected by any pump light that had arrived more than about $\tau_{D\text{-}F}$ seconds earlier than the input signal to point z. Therefore, in the limit of very large pump widths, the important parameter is the peak power of the pump, which is lower for greater pump widths in order to maintain the area or energy of the pump pulse. On the other hand, the gain also decreases when the pulse width is comparable to the time required by population inversion to build up along z. As a consequence, there is a certain minimum pump width below which there are no significant gains with moderate pump energies (about one tenth of the optimum width in Fig. 6). This fact was also shown in Refs. [36,37]. Due to the peculiarities of POFs, whose typical fiber diameters are much larger than those of glass fibers, the achievement of gain using pump pulses of very large duration, or, equivalently, using continuous pump power, would require the use of pump lasers of high output power, because the necessary energy of the long pulses would be larger than the energy of the optimum-width pulses shown in Fig. 6, which is already quite large.

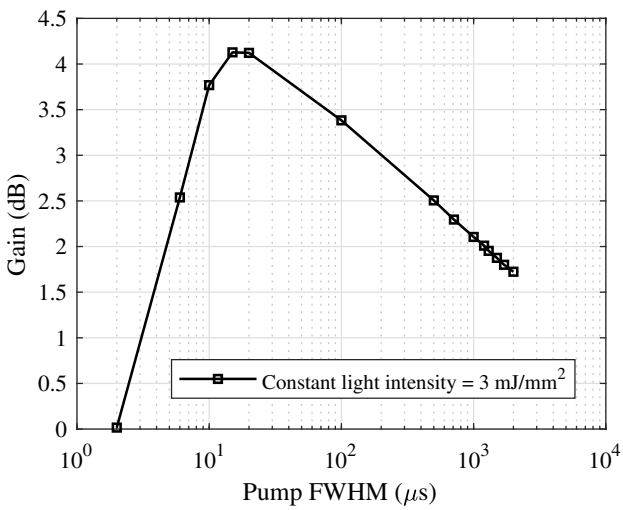

Fig. 6. Dependence of signal gain on the temporal width of the pump pulse for a constant pump energy density. General parameters as in Table 1. Fiber length: $L = 0.3$ m. Dopant concentration = 4000 ppm.

The gain is affected by signal width very slightly. For the calculations, we have used a width of 0.2 μs, but we have seen that the influence of this parameter is negligible as long as the signal is narrow enough for all of it to overlap in time with the highest pump powers of the pump pulse. For example, we have found a decrease in the gain of only 0.1 dB approximately if the signal width is increased from 0.2 μs to 2 μs for pump pulses of 15 μs. In contrast, the fiber length employed can be very influential, due mainly to the limited penetration of the pump power into the fiber until it becomes negligible as a consequence of the large absorption at the pump wavelength. If the fiber is shorter than this penetration distance, signal gain can be greatly reduced due to the shorter length available for stimulated emissions. Even if the fiber is longer than this penetration distance, signal gain is also affected by fiber length, albeit more slightly, owing to the material absorption at signal wavelength and absence of stimulated emissions at the furthest points, where the pump power does not reach. The fiber length of interest is the one that maximizes signal gain, which will be called optimum fiber length. Figures 7 and 8 show, respectively, optimum fiber length for each pump width in Fig. 6 and comparison between gains at the optimum length and at a longer one. The same pump width that maximizes the gain also yields the largest optimum length.

Taking all these results into account, we will use the parameters in Table 1 for simulation of the AC46- and AC56-doped fibers with concentrations lower than 4000 ppm (50 ppm and 500 ppm), in order to analyze the effect of concentration and of attenuation at the pump and signal wavelengths, which differ from one dopant to the other.

The distinguishing features of each of the 50 ppm and 500 ppm samples analyzed in this section are summarized in Table 2. As can be noticed, the first two samples in Table 2 differ in both the value of α and in dopant concentration, which affects the pump attenuation coefficient α_p, whereas the last two differ in the value of α_p. As is well known, the value of α_p coincides with the factor multiplying P_p in Eq. (1), because pump absorption is caused mainly by the dopant. Attenuation α at the emission wavelength also depends on dopant concentration, due to scattering effects, and its

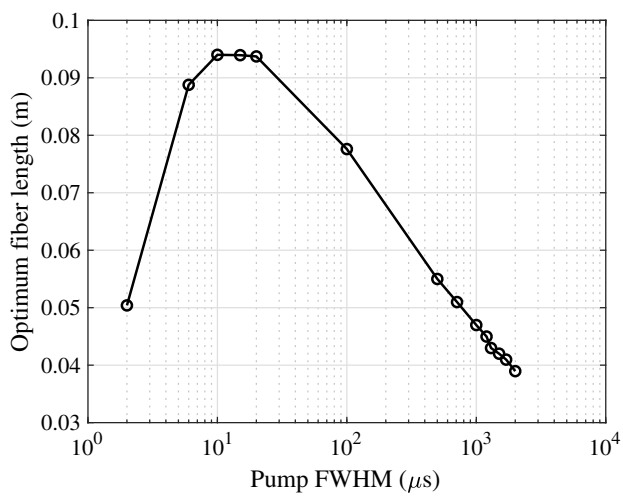

Fig. 7. Optimum fiber length for a constant pump energy density. General parameters as in Table 1. Dopant concentration = 4000 ppm.

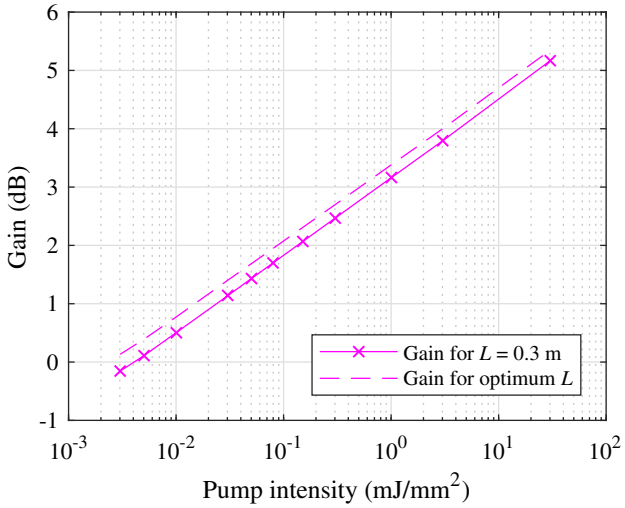

Fig. 8. Influence of using the optimum fiber length instead of a fixed one. General parameters as in Table 1. Fiber length: $L = 0.3$ m. Dopant concentration = 4000 ppm.

measurement is conditioned by fiber length, due to light leakage at the beginning of the fiber. For the fiber lengths employed in this work, we have measured the value of α as about 0.23 m^{-1}, i.e., 1 dB/m, in the 500 ppm samples, and slightly lower in the 50 ppm sample. We will also consider the hypothetical case in which α were negligible, which will serve us to clarify the individual influence of dopant concentration on the performance of a fiber amplifier based on these types of Eu-doped POFs. Comparing dopants allows the extrapolation of the qualitative results to other similar chelates of europium. However, the results are not merely qualitative. Even in quantitative terms, they are expected to be able to provide a gross estimate of the gain in each case, notwithstanding the limitations of any theoretical model (as already commented in Sections 1 and 2).

The evolution of $P(z)$, with $z = L$ (variable), along each of the two AC46 samples considered in Table 2 is shown in Figs. 9(a) and 9(b). As can be observed, employing a shorter fiber can serve to maximize the output power $P(z = L)$ when the attenuation coefficient α is not 0. This attenuation is the reason that $P(z)$ decreases from the length marked with "X" in Figs. 9(a) and 9(b), respectively. As can be noted, the value z of this mark is about 10 times smaller when the concentration is 10 times higher [Figs. 9(a) versus 9(b)], i.e., the value of z of that maximum is approximately inversely proportional to the concentration. The explanation is that the average distance between the dopant molecules is also divided by the same factor, while the molecules can still be assumed to act independently from one another due to the shielding of each europium ion by

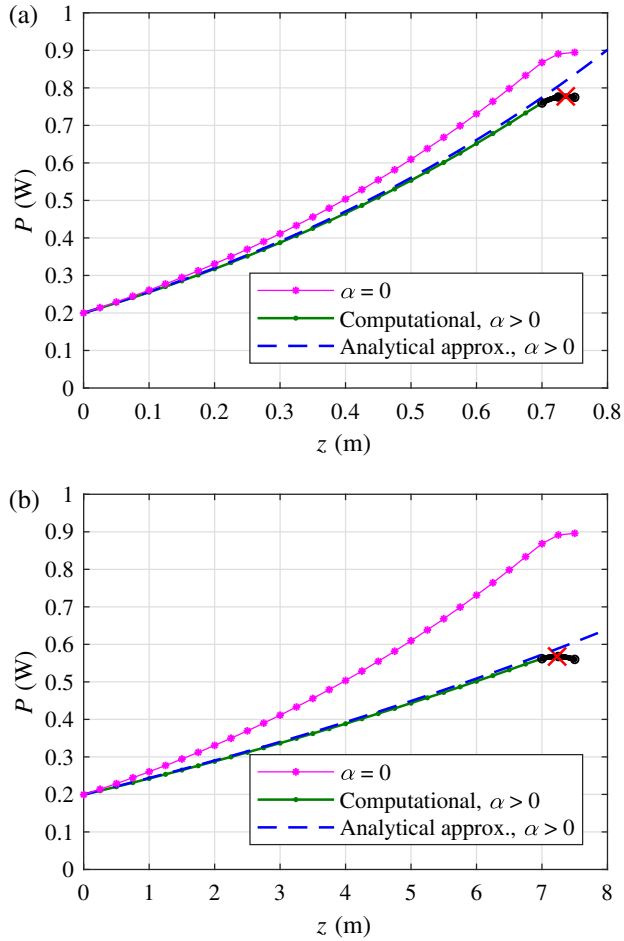

Fig. 9. Evolution of the generated power along the two AC46-doped POFs: (a) 500 ppm and (b) 50 ppm. Simulation parameters as in Tables 1 and 2. Solid line: computational results from the complete rate equations. Dashed line: results predicted by the simplified model formulated by Eq. (5). Point marked with "X": length for maximum $P(z)$, which is 0.736 m in (a) and 7.232 m in (b).

the surrounding ligands. In other words, the same absorption and emission phenomena occur in a shorter fiber length as long as the concentration is increased in the same proportion as L is reduced. However, this is only an approximate rule if the attenuation of P is not negligible, because, in a longer fiber, the signal undergoes relatively larger material absorption in the PMMA core. This PMMA attenuation also explains that the peak power $P(z = L)$ achieved is higher in the case in Fig. 9(a), corresponding to shorter maximum-power length than in the case in Fig. 9(b). A higher peak power also implies a higher gain in the energy of the signal pulse. Specifically, the calculated signal gains are 3.40 dB and 1.65 dB, respectively.

Table 2. Specific Differentiating Parameters of 50 ppm and 500 ppm Samples Considered for Theoretical Comparisons

Sample	N (molec./m^3)	α_p (dB/m) ($\lambda_p = 379$ nm)	α_p (m^{-1}) ($\lambda_p = 379$ nm)	α (m^{-1}) ($\lambda_s = 614$ nm)
Doped with 50 ppm AC46	$0.3 \cdot 10^{23}$	4.5	1.035	0.077
Doped with 500 ppm AC46	$3 \cdot 10^{23}$	45	10.35	0.23
Doped with 500 ppm AC56	$3 \cdot 10^{23}$	90	20.7	0.23

Moreover, maximizing the peak power of the output signal also serves to maximize signal gain when signal width is much narrower than pump width, because the signal pulse maintains its temporal shape (its proportions) along the final part of the fiber in such a case.

In order to be able to analytically quantify the differences in gain due to the presence or not of a non-zero signal attenuation coefficient α, we have also derived a simplified mathematical formula for $P(z)$ from the rate equations (see Appendix A). This formula is as follows:

$$P(z) = \frac{N_D(hc/\lambda_s)A_{\text{core}}\beta}{\tau_{D\text{-}F}(\sigma^e N_D - \alpha)}[\exp((\sigma^e N_D - \alpha)(z - z_0)) - 1], \quad \textbf{(5)}$$

where z_0 is a constant that is needed, in the presence of an input signal, for matching the value of P at $z = 0$ with the peak power of the input signal. Equation (5) shows that, at distances z in which the pump power is high enough to saturate N_D, $P(z)$ tends to increase in a nearly exponential way. Similarly, at distances z in which the pump power has already been attenuated to negligible values, i.e., where $N_D \approx 0$, $P(z)$ tends to diminish exponentially at a rate of α (m^{-1}) in stationary state. Between both ranges of distances, there is a progressive reduction in the slope of $P(z)$. For example, with the parameters corresponding to the first two samples in Table 2, it was computationally obtained, from the complete rate equations, that N_D remains saturated up to $z \approx 0.7$ cm and 7 cm, respectively. By applying Eq. (5) to these simulation conditions, it can be checked that the computational curves practically overlap with those predicted by the approximated analytical expression in the range of saturation distances of N_D [see the dashed lines in Figs. 9(a) and 9(b)]. Therefore, the results obtained from the numerical simulation of the model match the expected ones. Figure 9 also shows the disadvantage of using a fiber length that lies inside the range of saturation distances of N_D, because, in such a case, the corresponding exponential increase in P would be truncated as a consequence of reaching the end of the fiber, which would be highly influential on the final value $P(z = L)$ and, therefore, also on signal gain. The two samples in Figs. 9(a) and 9(b) differ in both dopant concentration and in α. We have repeated the calculations with $\alpha = 0$ [asterisk-marked lines in Figs. 9(a) and 9(b)], and the results confirm that $P(z = L)$ is exactly the same in both figures, and not only similar, as long as L is also scaled (divided) by the same factor multiplying N. Moreover, the gains in the signal energy also become equal if the aforementioned scale factor is applied to fiber length. For example, a gain of 4.15 dB is obtained at the lengths of maximum $P(z)$ for both figures.

The shape of $P(z)$ is strongly related to the penetration distance of pump power into the fiber. In order to gain insight into this shape, let us analyze the second and third samples in Table 2, which have identical dopant concentration N but different values of α_p for the same pump wavelength. In such conditions, the penetration distance of the pump is longer in the case of the sample with smaller α_p (i.e., the AC46-doped POF), which means that signal amplification can occur along a larger fiber length, which also contains more molecules of dopant when the concentration is the same. In consequence, a greater value of $P(z = L)$ is expected to be obtainable with the smaller value of α_p under the same pump conditions. This is corroborated in Fig. 10, in which the curve of $P(z)$ obtained for the AC56-doped POF does not reach as high as the maximum value of the curve for the AC46-doped POF, owing to the higher value of α_p in the AC56-doped fiber of the same concentration. This reasoning was also confirmed by calculating and comparing gains of the mentioned samples for different values of pump wavelengths. The results are shown in Fig. 11, in which we can see the gains corresponding to a fixed fiber length L (2 m), which is longer than, or equal to, the length beyond which $P(z)$ starts to decrease in each case. Such lengths range between 0.4 m and 2 m, as shown in the vertical axis in Fig. 12, and the value of α is 1 dB/m in both curves. As a consequence, the extra attenuation

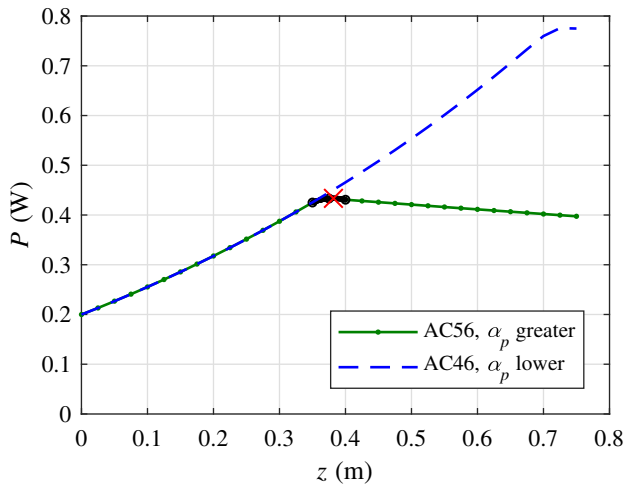

Fig. 10. Evolution of the generated power along the 500 ppm AC56-doped POF (solid line). Parameters as in Tables 1 and 2. Point marked with "X": length for maximum $P(z)$, which is 0.38 m. The power curve corresponding to the 500 ppm AC46-doped POF is also included.

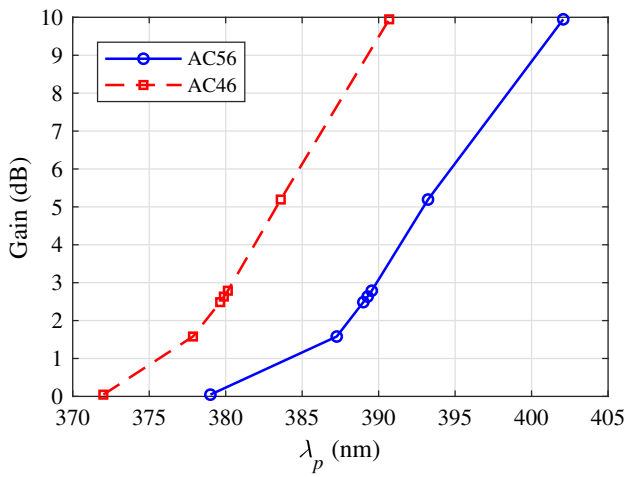

Fig. 11. Gains calculated for multiple pump wavelengths maintaining the fiber length L (2 m), which is greater than or equal to the optimum one in all cases. The solid line corresponds to the AC56-doped POF, whose α_p is higher, and the dashed line to the AC46-doped POF, whose α_p is lower. The dopant concentration is 500 ppm in both cases.

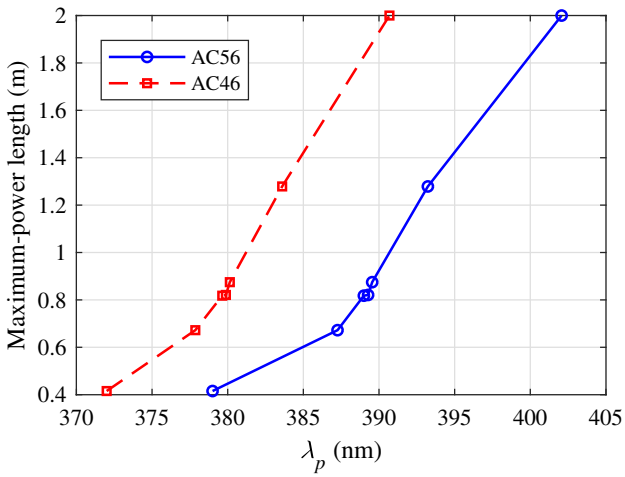

Fig. 12. Lengths that maximize the peak of the output power for each of the two 500 ppm-doped fibers in Table 2, calculated for multiple pump wavelengths. Remaining simulation parameters as in Table 1.

of emission power along the excess in length that attenuates $P(z)$ is in the range between 1.6 dB (when $z = 0.4$ m for the maximum P) and 0 dB (2 m). Figure 11 shows that, unless the fiber length is exaggeratedly large, the penetration distance of pump power is more influential on signal gain than the excess in length. For example, the gain is much higher, even by nearly 7 dB, at 390 nm in the fiber of longer pump penetration distance (i.e., the AC46-doped one). Therefore, if we have two fibers that differ only in the value of α_p, choosing the one of lower α_p is generally the best option. The only condition is that the fiber length employed has to be, at least, the length that maximizes $P(z)$. However, since α is not negligible, it is also true that employing greater dopant concentrations serves to reduce fiber length and, with this, the effect of α as well, which is detrimental also in the interval of lengths where $P(z)$ grows, as can be noticed from Eq. (5).

6. CONCLUSIONS

The authors present a model that serves to calculate the behavior in space and time of emission power in europium-chelate-doped POFs and its numerical solution by means of finite differences. This model is applied to the case of launching Gaussian pulses of signal and pump power at the input end of a fiber. Results confirm the existence of an optimum temporal width of the pump pulse that maximizes the gain for constant pump energy. This width is between 10 μs and 100 μs in our case, which is a fraction of the decay time of the europium ion. The model is applied to samples differing in dopant concentration and/or spectral attenuation. Results show the feasibility of applying a scale factor for calculation of the gain and maximum-power length when the dopant concentration is multiplied by the same factor. As for the pump attenuation coefficient α_p, it is shown that a fiber of lower α_p is generally the best option, on condition that the doped optical fiber utilized is long enough. It is also shown to what extent employing a greater dopant concentration serves to reduce the detrimental effect on the gain of attenuation at the emission wavelength. The qualitative reliability of some of the results presented in this paper is confirmed by means of a simplified analytical expression. The fact of having obtained a value similar to that measured in similar experiments reflects credit even on the quantitative reliability of the model. The results presented in this paper can provide valuable help with the experimental design of photonic devices based on these types of fibers.

APPENDIX A

From Eq. (3) in stationary state, and if N_D is approximately constant,

$$\frac{dP}{dz} = (\sigma^e N_D P - \alpha)P + \frac{N_D}{\tau_{D-F}} h \frac{c}{\lambda_s} \beta A_{\text{core}}.$$

Calling k_1 and k_2 the factor multiplying P and the second summand, respectively,

$$\frac{dP}{dz} = k_1 P + k_2.$$

Its analytical solution is (writing "≈" because k_1 and k_2 are only approximately constant)

$$P(z) \approx \frac{-k_2}{k_1} + C_1 \exp(k_1 z),$$

where C_1 is an arbitrary constant to be determined. In the case in which $P(0) = 0$, we have

$$P(z) = \frac{N_D (hc/\lambda_s) A_{\text{core}} \beta}{\tau_{D-F}(\sigma^e N_D - \alpha)} [\exp((\sigma^e N_D - \alpha)z) - 1].$$

Funding. European Regional Development Fund (ERDF); Ministerio de Economía y Competitividad (MINECO) (TEC2015-638263-C03-1-R); Eusko Jaurlaritza (ELKARTEK KK-2016/0030, ELKARTEK KK-2016/0059, ELKARTEK KK-2017/00033, ELKARTEK KK-2017/00089, IT933-16).

REFERENCES

1. Y. Koike, *Fundamentals of Plastic Optical Fibers* (Wiley, 2015).
2. M. G. Kuzyk, U. Paek, and C. Dirk, "Guest-host polymer fibers for nonlinear optics," Appl. Phys. Lett. **59**, 902–904 (1991).
3. C. Jiang, M. G. Kuzyk, J.-L. Ding, W. E. Johns, and D. J. Welker, "Fabrication and mechanical behavior of dye-doped polymer optical fiber," J. Appl. Phys. **92**, 4–12 (2002).
4. P. Miluski, M. Kochanowicz, J. Zmojda, and D. Doroszb, "Properties of Eu^{3+} doped poly(methyl methacrylate) optical fiber," Opt. Eng. **56**, 027106 (2017).
5. I. Parola, E. Arrospide, F. Recart, M. A. Illarramendi, G. Durana, N. Guarrotxena, O. García, and J. Zubia, "Fabrication and characterization of polymer optical fibers doped with perylene-derivatives for fluorescent lighting applications," Fibers **5**, 28 (2017).
6. I. Parola, D. Zaremba, R. Everta, J. Kielhorna, F. Jakobs, M. A. Illarramendi, J. Zubia, W. Kowalsky, and H.-H. Johannes, "High performance fluorescent fiber solar concentrators employing double-doped polymer optical fibers," Solar Energy Mater. Sol. Cells **178**, 20–28 (2018).
7. I. Parola, M. A. Illarramendi, J. Arrue, I. Ayesta, F. Jiménez, J. Zubia, A. Tagaya, and Y. Koike, "Characterization of the optical gain in doped polymer optical fibres," J. Lumin. **177**, 1–8 (2016).

8. J. Arrue, F. Jiménez, I. Ayesta, M. A. Illarramendi, and J. Zubia, "Polymer-optical-fiber lasers and amplifiers doped with organic dyes," Polymers **3**, 1162–1180 (2011).
9. M. A. Illarramendi, J. Arrue, I. Ayesta, F. Jiménez, J. Zubia, I. Bikandi, A. Tagaya, and Y. Koike, "Amplified spontaneous emission in graded-index polymer optical fibers: theory and experiment," Opt. Express **21**, 24254–24266 (2013).
10. J. He, W.-K. E. Chan, X. Cheng, M.-L. V. Tse, C. Lu, P.-K. A. Wai, S. Savovic, and H.-Y. Tam, "Experimental and theoretical investigation of the polymer optical fiber random laser with resonant feedback," Adv. Opt. Mater. **6**, 1701187 (2018).
11. S. Abrate, *Handbook of Fiber Optic Data Communication: A Practical Guide to Optical Networking*, C. DeCusatis, ed., 4th ed. (Elsevier, 2013), pp. 37–54.
12. A. N. Z. Rashed, A. E.-N. A. E. G. Mohamed, S. A. E. R. S. Hanafy, and M. H. Aly, "A comparative study of the performance of graded index perfluorinated plastic and alumino silicate optical fibers in internal optical interconnections," Optik **127**, 9259–9263 (2016).
13. A. Tagaya, Y. Koike, E. Nihei, S. Teramoto, K. Fujii, T. Yamamoto, and K. Sasaki, "Basic performance of an organic dye-doped polymer optical fiber amplifier," Appl. Opt. **34**, 988–992 (1995).
14. A. Tagaya, S. Teramoto, T. Yamamoto, K. Fujii, E. Nihei, Y. Koike, and K. Sasaki, "Theoretical and experimental investigation of rhodamine B-doped polymer optical-fiber amplifiers," IEEE J. Quantum Electron. **31**, 2215–2220 (1995).
15. G. D. Peng, P. L. Chu, Z. Xiong, T. W. Whitbread, and R. P. Chaplin, "Dye-doped step-index polymer optical fiber for broadband optical amplification," J. Lightwave Technol. **14**, 2215–2223 (1996).
16. M. Karimi, N. Granpayeh, and M. Moravvej-Farshi, "Analysis and design of a dye-doped polymer optical fiber amplifier," Appl. Phys. B **78**, 387–396 (2004).
17. J. Clark, L. Bazzana, D. D. C. Bradley, J. Cabanillas-Gonzalez, G. Lanzani, D. G. Lidzey, J. Morgado, A. Nocivelli, W. C. Tsoi, T. Virgili, and R. Xia, "Blue polymer optical fiber amplifiers based on conjugated fluorene oligomers," J. Nanophoton. **2**, 023504 (2008).
18. J. Zubia and J. Arrue, "Plastic optical fibers: an introduction to their technological processes and applications," Opt. Fiber Technol. **7**, 101–140 (2001).
19. M. J. F. Digonnet, *Rare-Earth-Doped Fiber Lasers and Amplifiers, Revised and Expanded*, 2nd ed. (Marcel Dekker, Inc., 2001).
20. D. Oh, N. Song, and J.-J. Kim, "Plastic optical amplifier using europium complex," Proc. SPIE **4282**, 1–9 (2001).
21. R. Caspary, S. Möhl, A. Cichosch, R. Evert, S. Schütz, and H.-H. Johannes, "Eu-doped polymer fibers," in *15th International Conference on Transparent Optical Networks (ICTON)* (2013), pp. 1–4.
22. K. Nakamura, Y. Hasegawa, H. Kawai, N. Yasuda, Y. Tsukahara, and Y. Wada, "Improvement of lasing properties of europium (III) complexes by increase of emission quantum yield," Thin Solid Films **516**, 2376–2381 (2008).
23. H. Liang, F. Xie, M. Liu, Z. Jin, F. Luo, and Z. Zhang, "Luminescence studies of europium chelates with increasing benzene ring substituents ligand-doped polymer," Spectrochim. Acta A **71**, 588–591 (2008).
24. H. Liang and F. Xie, "Photoluminescence study of a europium (III) complex containing 1, 5-styrylacetylacetone ligands," Spectrochim. Acta A **77**, 348–350 (2010).
25. K. Kuriki and Y. Koike, "Plastic optical fiber lasers and amplifiers containing lanthanide complexes," Chem. Rev. **102**, 2347–2356 (2002).
26. G. F. de Sá, O. L. Malta, C. de Mello Donegá, A. M. Simas, R. L. Longo, P. A. Santa-Cruz, and E. F. da Silva, Jr., "Spectroscopic properties and design of highly luminescent lanthanide coordination complexes," Coord. Chem. Rev. **196**, 165–195 (2000).
27. H. Samelson, A. Lempicki, C. Brecher, and V. Brophy, "Room-temperature operation of a europium chelate liquid laser," Appl. Phys. Lett. **5**, 173–174 (1964).
28. A. Tagaya, Y. Koike, T. Kinoshita, E. Nihei, T. Yamamoto, and K. Sasaki, "Polymer optical fiber amplifier," Appl. Phys. Lett. **63**, 883–884 (1993).
29. C. Koeppen, S. Yamada, G. Jiang, A. F. Garito, and L. R. Dalton, "Rare-earth organic complexes for amplification in polymer optical fibers and waveguides," J. Opt. Soc. Am. B **14**, 155–162 (1997).
30. H. Liang, Q. Zhang, Z. Zheng, H. Ming, Z. Li, J. Xu, B. Chen, and H. Zhao, "Optical amplification of $Eu(DBM)_3$Phen-doped polymer optical fibers," Opt. Lett. **29**, 477–479 (2004).
31. H. Liang, B. Chen, Q. Zhang, Z. Zheng, H. Ming, and F. Guo, "Amplified spontaneous emission of $Eu(DBM)_3$phen doped step-index polymer optical fiber by end-pumping with a YAG," J. Appl. Polym. Sci. **98**, 912–916 (2005).
32. Z. Zheng, H. Ming, X. Sun, J. Yang, D. Zhang, and J. Xie, "Study of Eu $(DBM)_3$phen-doped optical polymer waveguides," J. Opt. Soc. Am. B **22**, 820–824 (2005).
33. K. Kuriki, S. Nishihara, Y. Nishizawa, A. Tagaya, Y. Okamoto, and Y. Koike, "Fabrication and optical properties of neodymium-, praseodymium- and erbium- chelates-doped plastic optical fibres," Electron. Lett. **37**, 415–417 (2001).
34. T. Kobayashi, K. Kuriki, S. Nishihara, Y. Okamoto, and Y. Koike, "Rare earth-doped polymer optical fibers for optical amplification," Proc. SPIE **3942**, 158–166 (2000).
35. O. L. Malta, H. F. Brito, J. F. S. Menezes, F. R. Gonçalves e Silva, C. de Mello Donegá, and S. Alves, Jr., "Experimental and theoretical emission quantum yield in the compound Eu(thenoyltrifluoroacetonate)$_3$.2(dibenzyl sulfoxide)," Chem. Phys. Lett. **282**, 233–238 (1998).
36. I. Ayesta, "Study of active polymer optical fibres to improve their performance as lasers and amplifiers," Ph.D. thesis (University of the Basque Country UPV/EHU, 2013).
37. I. Ayesta, F. Jiménez, J. Arrue, J. Zubia, and M. A. Ilarramendi, "Polimerozko zuntz optiko dopatuen erabilera, laser eta anplifikagailu gisa," EKAIA ale berezia (special volume), 121–135 (2015).